

KNOT INVARIANTS AND THEIR RELATIONS: A TOPOLOGICAL PERSPECTIVE

PAWEŁ DŁOTKO, DAVIDE GURNARI, AND RADMILA SAZDANOVIC

ABSTRACT. This work brings methods from topological data analysis to knot theory and develops new data analysis tools inspired by this application. We explore a vast collection of knot invariants and relations between them using Mapper and Ball Mapper algorithms. In particular, we develop versions of the Ball Mapper algorithm that incorporate symmetries and other relations within the data, and provide ways to compare data arising from different descriptors, such as knot invariants. Additionally, we extend the Mapper construction to the case where the range of the lens function is high dimensional rather than a 1-dimensional space, that also provides ways of visualizing functions between high-dimensional spaces. We illustrate the use of these techniques on knot theory data and draw attention to potential implications of our findings in knot theory.

1. INTRODUCTION

Classification of knots and links, while interesting on its own, also provides insights into classification of 3- and 4-dimensional manifolds [36, 31] due to classical theorems such as the Lickorish-Wallace theorem and other, more recent, results. Knots and links also play an important role in physics, biology, and other sciences. Classification of knots uses a wide array of techniques from different areas of mathematics, for example, to derive knot invariants. In 1998 just over 1.7 million knots were tabulated by Hoste, Thistlethwaite, and Weeks [23, 22]. The number of tabulated knots rose up to 350 million in 2019 due to work of Burton [8, 7] and contains all knots with fewer than 20 crossings. Since the number of knots with a given number of crossings grows exponentially [14] warranting the use of big data techniques [24, 26, 40, 30].

However, using big data techniques poses new questions such as: "What is the best way to represent knots as input for different big data techniques?" and "How to get a representative sample of the infinite space of knots and links?". Our answer to the first question is to use various knot invariants, such as the Alexander, Jones, HOMFLYPT, and Khovanov polynomials. It should be noted that despite using multiple invariants, they fail to distinguish all knots, even if combined. It is even unknown if there is a non-trivial knot that has the same Jones polynomial as the unknot. However this is the most viable approach that provides a good approximation of the space of knots and allows for explorations of knot invariants and their relations.

When it comes to randomness and sampling, while there have been significant results, e.g., [13, 9], in this paper we consider all knots with at most 15 to 17 crossings, as our results appear to be stable with respect to the filtration by the number of crossings. This collection of knots is not a finite random uniform sample for a number of reasons. For example, alternating knots are over-represented in this collection but other biases might also introduce a systematic error in our explorations.

Date: September 3, 2021.

PD and DG acknowledges support by Dioscuri program initiated by the Max Planck Society, jointly managed with the National Science Centre (Poland), and mutually funded by the Polish Ministry of Science and Higher Education and the German Federal Ministry of Education and Research.

RS was partially supported by NSF grant DMS-185470.

In this paper we are using existing and developing new methods from Topological Data Analysis (TDA) to understand global properties of the space of knots up to 17 crossings. Note that the applicability of developed techniques is not restricted to knot theory or to data coming from theoretical computations. In particular, we adapt and combine the Mapper [39] and Ball Mapper [33] algorithms to the context of knot invariants, taking into account their special properties, such as those that induce symmetries of the corresponding point cloud, and providing new tool for analyzing their structure and relations between different invariants.

The paper is organized as follows. Section 2 provides the necessary background on Mapper and Ball Mapper algorithms, as well as a survey of necessary notions in knot theory. Section 3 describes a way to turn knot invariants into point clouds so they can be analyzed by TDA techniques. Section 4 focuses on adaptations and new developments of Mapper algorithms that are applicable to any point cloud. In Section 4.1 we develop a version of Ball Mapper that takes into account symmetries (global or partial) of the data. Section 4.2 describes a way to construct mapper graphs for lens functions with very high dimensional domains and codomains. Lastly, in Section 4.3 we discuss how to combine the strengths of Mapper and Ball Mapper algorithms to analyze data, relations between high dimensional point clouds, and visualize maps between different data sets. Section 5 present the results of application of the the presented Mapper-type techniques to the space of knots and their invariants, while Section 6 focuses on the comparison of knot invariants using techniques from Section 4.3.

ACKNOWLEDGEMENTS

The authors want to thank Alexander Shumakovitch for providing the data for the Rasmussen s-invariant and Khovanov homology used in this paper and Adam Lowrance for insightful comments.

2. BACKGROUND

In this section we present the standard tools of Topological Data Analysis: the Mapper algorithm [39] as well as more recent Ball Mapper [33]. In addition we introduce standard topics in knot theory that are used in this paper.

2.1. Mapper. *Mapper algorithm*, introduced in 2007 in [39], is one of the most recognized tools of Topological Data Analysis. Its construction is made in a number of steps; Let us have a collection of points X , typically embedded in some high dimensional space, as well as a function $f : X \rightarrow \mathbb{R}^n$, referred to as *lens function*. Typically, $n = 1$ is used. We cover the range $f(X) \subset \mathbb{R}^n$ by an *overlapping cover* \mathcal{C} . For $n = 1$, \mathcal{C} may consist of k intervals covering $f(X)$ having property that two constitutive intervals overlap on p percent of their length. The two parameters: *the number of intervals* (k) and the *overlapping percentage* (p) are typical input parameters of the Mapper algorithm.

For each interval $I \in \mathcal{C}$, take $f^{-1}(I) \subset X$ and search for the clusters therein. The clustering algorithm used for that purpose is yet another parameter of the Mapper construction. For $I \in \mathcal{C}$ let C_I indicate the collection of clusters found in $f^{-1}(I)$. Each cluster in $\bigcup_{I \in \mathcal{C}} C_I$ will correspond to a vertex of the abstract graph $G = (V, E)$. Given a cluster $A \in C_I$, the vertex corresponding to A is denoted by $v(A)$. Undirected edges of the graph G are placed between any two vertices $v(A)$ and $v(B)$ corresponding to clusters $A \in C_I$ and $B \in C_J$, for $I, J \in \mathcal{C}$ if and only if $A \cap B \neq \emptyset$. The resulting graph $G = (V, E)$ will be called a *Mapper graph*.

The idea of the Mapper construction is given at the Figure 1. The graph G can be additionally colored by a function of interests. Suppose that we are given a function $g : X \rightarrow \mathbb{R}$. We define an *induced function* $\hat{g} : G \rightarrow \mathbb{R}$, where G is the Mapper graph defined above. Since each vertex $v(A)$ in G correspond to a cluster $A \in \bigcup_{I \in \mathcal{C}} C_I$, we define $\hat{g}(v(A)) = \frac{\sum_{x \in A} g(x)}{|A|}$, i.e. take an averaged value

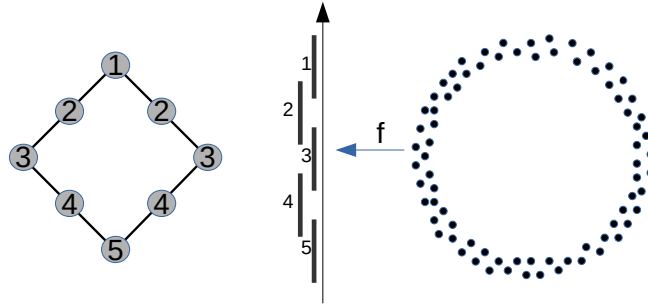


FIGURE 1. Mapper construction illustration. As an input, use the two dimensional point cloud X in a shape of a circle shown on the right. The function $f : X \rightarrow \mathbb{R}^1$ is a projection of a point to its second coordinate. We cover the range of f with five intervals, enumerated from 1 to 5 then compute the inverse image of each interval. In this example, the inverse images of intervals 1 and 5 contain one cluster, while inverse images of intervals 2, 3 and 4 contain two clusters each. Moreover there are obvious connections between the clusters in the inverse image of intervals i and $i + 1$ for $i \in 1, 2, 3, 4$. They give rise to edges in the Mapper graph presented on the left. Note that the (non-unique) enumeration of vertices comes from the enumeration of elements of the cover \mathcal{C} .

of a function g on the cluster A as the value of the induced function on the vertex corresponding to A . This induced function is subsequently visualized using a color scale.

2.2. Ball Mapper. A *Ball Mapper Algorithm* introduced in [33] is an attempt to obtain a cover of the input collection of points X , similar to the one that is obtained in the Mapper algorithm, in a conceptually simpler way. Starting from a point cloud X , and a constant $\epsilon > 0$, a subset $L \subset X$ is selected having the property that for every $x \in X$ there exist $l \in L$ such that $d(x, l) \leq \epsilon$. Such a subset L is called *an ϵ net* of X . Algorithm 1 is a greedy algorithm to compute an ϵ net.

Data: Point cloud X , $\epsilon > 0$

Result: $L \subset X$, an ϵ -net

$L = \emptyset$

while *There exist a point $x \in X$ farther than ϵ from every point in L* **do**

$| L = L \cup x$

end

return L

Algorithm 1: Greedy ϵ -net algorithm [33].

Note that $X \subset \bigcup_{l \in L} B(l, \epsilon)$. The *Ball Mapper graph* is obtained by assigning each ball $B(l, \epsilon)$ with a vertex $v(l)$ of the graph, and by placing an edge between any two vertices whose corresponding balls jointly cover points from X . An idea of the Ball Mapper algorithm, for the dataset from Figure 1, is presented at the Figure 2.

Analogously to Mapper graphs, Ball Mapper graphs can also be used to visualize a function of interests. Given $f : X \rightarrow \mathbb{R}$, we define an *induced function* $\hat{f} : G \rightarrow \mathbb{R}$ on the Ball Mapper graph G in the following way; every vertex $v(l)$ in G gets the value $\hat{f}(v(l)) = \frac{\sum_{x \in B(l, \epsilon) \cap X} f(x)}{|B(l, \epsilon) \cap X|}$. The induced function \hat{f} is subsequently visualized with a color scale. Both in case of induced functions

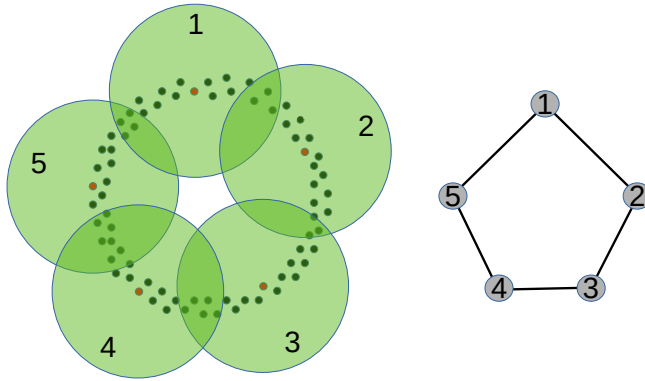


FIGURE 2. Ball Mapper algorithm- an illustration. Using the point cloud X in the Figure 1 we first select an ϵ -net (red points in the left figure). Construct balls of radius ϵ centered in all the points of the net (green). The union of those balls provides a cover of our data space. Ball Mapper is a one dimensional nerve of the obtained cover. In more detail, to each ball $B(A, \epsilon)$ we assign a vertex $v(A)$ in the abstract graph $G = (V, E)$. Two balls $B(N, \epsilon)$ and $B(K, \epsilon)$ that jointly cover some points from X give rise to an edge between $v(N)$ and $v(K)$. The Ball Mapper graph of this cover is shown on the right with the corresponding balls and vertices labeled with the same number.

on Mapper and Ball Mapper graphs it is a good practice to check the *variation of the values of f* on each element of the cover and compare it to the value of the induced function. The variation should ideally be small compared to the function value. In this case, the induced function \hat{f} can be considered a good approximation of the function f .

2.3. Knot theory: brief introduction. A knot is a class of embeddings of S^1 into \mathbb{R}^3 up to isotopy. Although knots naturally live in 3-dimensional space, usually they are represented as planar drawings referred to as knot diagrams [25, 32], see Figure 3. A knot diagram is a projection of a knot on some plane such that no three points on the knot project to the same point and if two points project to the same point, called a crossing, we keep track on their distance to the plane by recording which strand was on top and which on the bottom Figure 4. Working with knot diagrams brings the benefits of working in the plane with 4-valent graphs with the additional information at the vertices, at the inconvenience of having infinitely many diagrams of any knot. As a geometric objects, knots are hard to study - it is not easy to determine if two given embeddings are isotopic. There is no good notion of proximity between knots available. Consequently, a number of *knot invariants*, have been introduced in an attempt to compare knots. Knot invariant is a quantity such as number, polynomial, group or a homology theory, such that if two knots are the same (isotopic) they have the same invariant. In this paper we focus on the following knot invariants:

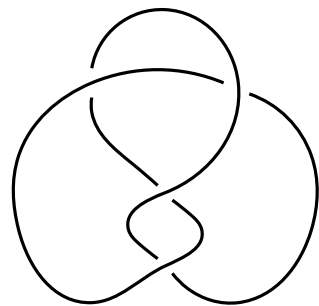


FIGURE 3. A diagram D of a trefoil knot denoted by 3_1 .

- Numerical: crossing number, signature denoted as $\sigma(K)$ [28] defined as a signature of a matrix obtained using a Seifert surface, Rasmussen s-invariant [35] derived from Khovanov homology and denoted by $s(K)$.
- Polynomial: Alexander $\Delta(K)(t)$ [2], Jones $J(K)(q)$ [27], $P(K)(a, z)$ HOMFLYPT [15], and Khovanov polynomial $Kh(K)(q, t)$ capturing the free part of Khovanov homology $Kh(K)$ that categorifies the Jones polynomial [29].

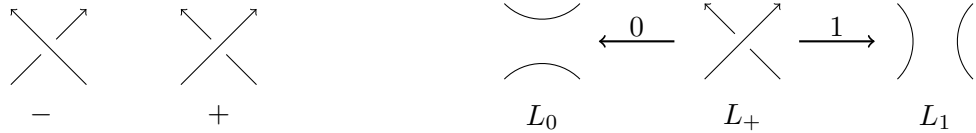


FIGURE 4. Conventions for crossings and smoothings in link diagrams.

Instead of definitions for knot invariants that often rely on advanced algebraic, geometric and combinatorial topology, we provide references, such as [32, 36, 31] and key insights that allow us to analyze these knot invariants and their relations. HOMFLYPT is the most general polynomial satisfying a skein relation [15, 34] written following conventions from Figure 4. More precisely we are considering oriented knots L_+ , L_- , and L_1 that differ only at one crossing where L_+ , and L_- have positive and negative crossings and link L_1 has an oriented smoothing depicted as L_1 in Figure 4:

$$(1) \quad aP(L_+) + \frac{1}{a}P(L_-) = zP(L_1)$$

HOMFLYPT specializes to the Jones polynomial [27] by substituting $a = t^{-1}$ and $z = \sqrt{t} - \frac{1}{\sqrt{t}}$ and to Alexander polynomial [2] by substituting $a = 1$ and $z = \sqrt{t} - \frac{1}{\sqrt{t}}$.

On the other hand, Khovanov homology $KH^{i,j}(K)$ is a bigraded homology theory that categorifies Jones polynomial [29] and Khovanov polynomial is the Poincare polynomial of this homology theory

$$(2) \quad Kh^{i,j}(K)(q,t) = \sum_{i,j} t^i q^j \dim_{\mathbb{K}} H^{i,j}(K)$$

TABLE 1. Values of several knot polynomials for the unknot and the trefoil and the corresponding data vector. Note that for the 2-variable polynomial the matrix is flattened into a vector; for the HOMFLYPT variable z is in rows, a in columns, and for the Khovanov q is in rows and t in columns.

In particular, Jones polynomial [27] can be obtained from Khovanov polynomial via the following relation $(q + \frac{1}{q})J(K)(q^2) = Kh(K)(-1, q)$.

The relations between these invariants are really interesting and not fully understood. For example, for alternating knots Jones polynomial and signature determine Khovanov polynomial [17].

while it is known that Khovanov homology is stronger invariant than the Jones polynomial. Signature and Rasmussen s-invariant often coincide and both provide a lower bound on the unknotting number. It is natural to expect that they can be different for knots with higher unknotting numbers.

For each knot K one can consider its mirror denoted by $\text{mir}(K)$, obtained by switching all positive and negative crossings in the knot diagram of K . It is common for knot tables to contain only one knot from each pair $(K, \text{mir}(K))$, since many of the invariants are the same for K and $\text{mir}(K)$ or there is a straightforward relation between the two values. While Alexander polynomial does not distinguish between the knot and its mirror, for the Jones polynomial we have that [31, 27]

$$(3) \quad J(\text{mir}(K))(q) = J(K)(q^{-1}),$$

For the signature [31],

$$(4) \quad \sigma(\text{mir}(K)) = -\sigma(K)$$

for Khovanov polynomial,

$$(5) \quad Kh(q^{-1}, t^{-1})(\text{mir}(K)) = Kh(q, t)(K)$$

for HOMFLYPT polynomial,

$$(6) \quad P(\text{mir}(K))(a, z) = P(K)(a^{-1}, z)$$

for the Rasmussen s-invariant [35]

$$(7) \quad s(\text{mir}(K)) = -s(K).$$

Note that the absolute values of signature and Rasmussen s-invariant of alternating knots coincide, and that absolute values of both provide lower bounds on the unknotting number. Moreover, Note that Khovanov width is related to the Turaev genus $g_T(K)$: $\frac{1}{2}|\sigma(K) - s(K)| \leq g_T(K)$ [12]. There are other invariants that can be derived from Khovanov homology such as its width or the page on which various spectral sequences collapse that can also be related to the unknotting number and other numerical invariants [3, 4, 5, 10]. Khovanov width $w_{KH}(K)$ is equal to the largest horizontal distance between two lines of slope two that contain non-trivial Khovanov homology groups [29].

3. KNOT DATA

3.1. Knot invariant computations. The knot invariants considered in this paper include Khovanov homology, Jones, Alexander, and HOMFLYPT polynomials, minimal crossing number, whether a knot is alternating or non-alternating, signature and the Rasmussen invariant. The data analyzed in this paper was created by J.S. Levitt, A. Shumakovitch and D. Gurnari and it is freely available at [21]. The first data set containing Jones and Alexander polynomials of knots up to 17 crossings and their numerical invariants listed above, as well as HOMFLYPT polynomial of all knots up to 15 crossings were computed by J. S. Levitt using the Knot Theory package [6]. For a given polynomial invariant, each knot is represented by a coefficient vector. A detailed description of how to construct such vectors is provided in [30].

Rational Khovanov homology computations, referred to as the Khovanov polynomial throughout the paper, and the Rasmussen invariant of all knots up to 13 crossings and all non-alternating knots with 14-15 crossings were done by A. Shumakovitch [37]. Khovanov polynomials are provided in PARI/GP format. For the purpose of this work each Khovanov polynomial has been converted to a coefficient vector using the Python to PARI interface CyPari2 [1]. Additions specific to this paper, provided by D. Gurnari, deal with the choice of knot and its mirror, and the consistent ordering of data within different knot invariant clouds, which is essential for results presented in Section 6.

3.2. From knot invariants to point clouds. In this paper we introduce a novel idea of creating point clouds associated with knots and link in order to be able to analyze the space of knots using ideas from topological data analysis. In particular, we focus on creating and analyzing point clouds corresponding to one- and two-variable polynomial invariants of knots and links

Given a finite collection of knots \mathcal{K} , first we construct a point cloud $\mathcal{I}(\mathcal{K})$ corresponding to the coefficients of the one-variable polynomial invariant \mathcal{I} , in the following way:

Step 1 Given a knot $K \in \mathcal{K}$ and its single variable polynomial $I(K)$ extract a vector of the coefficients.

Step 2 Compute the minimal and maximal powers \min_t, \max_t of the variable denoted by t among all knots in \mathcal{K} . Then the maximal length of all considered vectors is $d = \max_t - \min_t + 1$.

Step 3 Add zeros on both sides of each vector of coefficients to obtain a vector $I(K)_v \in \mathbb{R}^d$ to ensure a correct alignment of corresponding powers.

Note that in this way all vectors are of the same length determined by the overall minimum and maximum exponent, and, the coefficients of a given power are in the same position in the vector for all the considered knots.

In case we have a two-variable polynomial, such as Khovanov or HOMFLYPT, we apply Steps 1-3, as described above, in the case of one-variable polynomial, to both variables. In this way we first obtain a matrix padded with zeros, and create a corresponding vector by linearizing this matrix by concatenating its rows. These vectors live in \mathbb{R}^d where $d = (\max_p - \min_p + 1)(\max_q - \min_q + 1)$ where p and q stand for the two variables in the corresponding polynomial.

Next, note that the Jones coefficient vector of its mirror is obtained by reversing the original vector, see (3), and therefore the point cloud admits a central reflection around the origin. The HOMFLYPT coefficient matrix of the mirror knot can be obtained by reversing the columns of the original matrix (6). The Khovanov coefficient matrix of the mirror knot can be obtained by reversing both rows and columns (5).

Note that considering both knots and their mirrors increases the dimension of the coefficient vectors. For example, in the case of Jones polynomials $\min_t(\text{mir}(K)) = -\max_t(K)$ and $\max_t(\text{mir}(K)) = -\min_t(\text{mir}(K))$ as a consequence of relation (3). The coefficient vectors will then live in \mathbb{R}^d where $d = 2\max(|\max_t|, |\min_t|) + 1$.

4. NEW DEVELOPMENT OF MAPPER ALGORITHMS

In this section we describe an enhancement of the Ball Mapper algorithm that enables dealing with perceived or assumed symmetries of the point clouds, see Subsection 4.1. Later, subsection 4.2 provides a combination of Mapper and Ball Mapper approaches to enhance their strengths for data analysis. Finally, Subsection 4.3 provide visualizations of maps between high dimensional euclidean spaces.

4.1. Equivariant Ball Mapper. Suppose our data belongs to a metric space (X, d) with automorphism group H acting on it. In this paper we assume that for every $x \in X$ and for every $g \in H$, $g(x) \in X$, i.e. there is no noise in X , all the data is given exactly. This is the case for the integer-valued knot polynomials we consider. Note that since H is an automorphism group, we have that for every $x, y \in X$ and every $g \in H$, $d(x, y) = d(g(x), g(y))$. For every point $x \in X$, and isometry $g \in H$ the orbit $\Omega_g(x)$ of x will contains the sequence of points $x, g(x), g^2(x), \dots, g^n(x) \in X$. We assume that $g^{n+1}(x) = x$. Additionally we assume that the isometries of G are ordered and denote by $\Omega(x)$ the sequence of elements of orbits $\Omega_{g_i}(x)$, for all $g_i \in H$.

Jones polynomial data, with relation (3) ensuring that the point cloud is centrally symmetric with respect to the origin, provides a good example a dataset with a simple automorphism group, \mathbb{Z}_2 generated by the central reflection, acting on it.

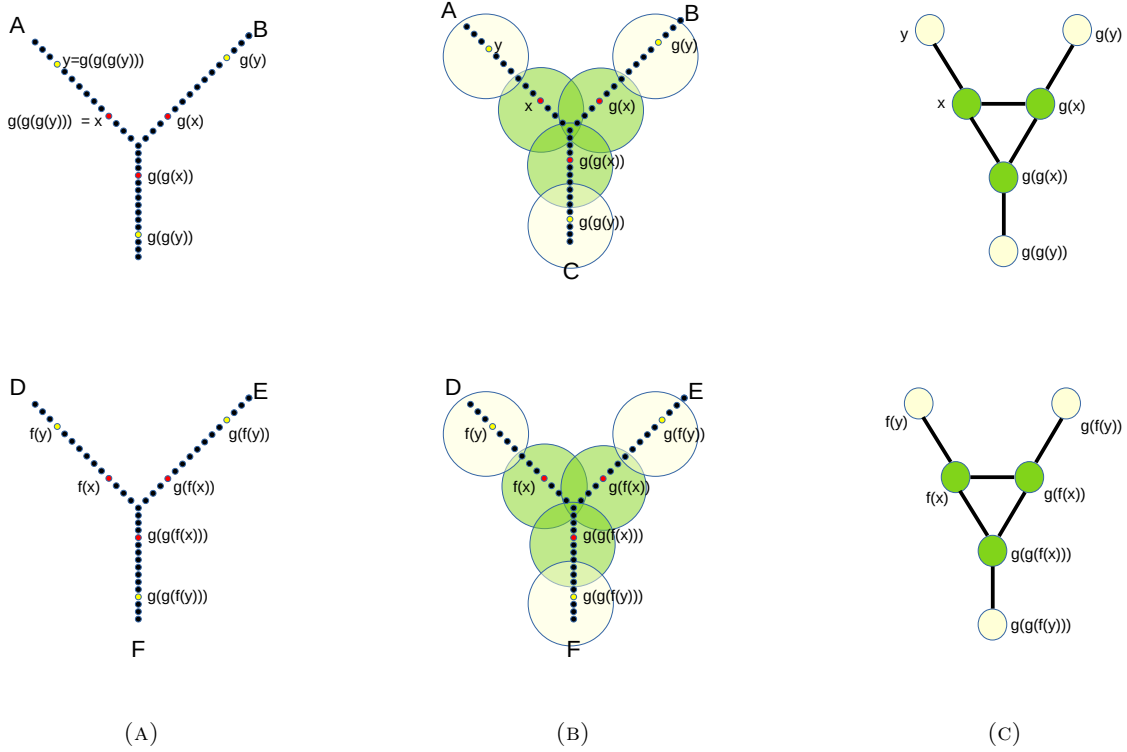


FIGURE 5. A point cloud X (column A) consisting of two copies of Y-shape sampled with a collection of points. The following transformations acts on X ; The transformation f maps points from one Y-shape to the corresponding points in the other Y-shape. In particular, branch A is mapped via f to D, B to E and C to F. The transformation g is a 120 degree rotation on each Y-shape. In particular, A is mapped via g to B, B to C, C to A, D to E, E to F and F to D. The orbit of points x and y via maps f and g are depicted. Points x and y , together with all elements of their orbits, form a collection of landmarks. The ϵ -radius balls centered in those points are shown in the second column (B). The last column (C) present an equivariant Ball Mapper graph which corresponds to the obtained cover and an induced action of f and g on the Ball Mapper graph.

Given a point cloud X and an automorphism group H acting on it, we modify the Ball Mapper algorithm in such a way that there is a *lift* of an action of H to the Ball Mapper graph G . This is how we understand the lift; given a vertex $v(l) \in G$ consider $B(l, \epsilon) \cap X$, i.e. all the points in X covered by a ball corresponding to $v(l) \in G$. Take $g \in H$. We require that all the points in $g(B(l, \epsilon) \cap X)$ are covered by a ball $B(g(l), \epsilon)$ and there are no other points in this ball. The vertex in G corresponding to the ball $B(g(l), \epsilon)$ will be then denoted by $\hat{g}(v(l))$. Note that \hat{g} , shadowing g , is acting on an abstract graph, and therefore certain properties of g will not be reflected in \hat{g} .

An example of the presented construction is given at the Figure 5.

To ensure the condition described above is satisfied, the procedure of selection of ϵ -net $L \subset X$ needs to be appropriately adjusted. In most of implementations L is chosen in the greedy way presented in Algorithm 1. Adjusting this Algorithm 1 so that the obtained ϵ -net L is invariant under the action of H amounts to Algorithm 2. The main idea is to add $\Omega_g(x) = \{g(x)\}_{g \in H}$ to

the constructed set of landmark points each time x is added there. This idea is formalized in the algorithm below;

```

Data: Point cloud  $X$ ,  $\epsilon > 0$ , group  $H$  acting on  $X$ 
Result:  $L \subset X$ , a  $H$ -equivariant  $\epsilon$ -net
 $L = \emptyset$ 
while There exist a point  $x \in X$  farther than  $\epsilon$  from any point in  $L$  do
|  $L = L \cup \Omega(x)$ 
end
return  $L$ 

```

Algorithm 2: Equivariant greedy ϵ -net.

Note that, in Algorithm 2, when a single point $x \in X$ is added to the ϵ -net L , then all of $\Omega(x)$ is added to L . Since each $g \in H$ is an isometry, for every $l \in L$, if $y \in B(l, \epsilon) \cap X$, $g(y) \in B(g(l), \epsilon) \cap X$. As each $B(l, \epsilon) \cap X$ corresponds to a vertex in the Ball Mapper graph, and the action of H on X is lifted to vertices of the Ball Mapper graph as described above.

4.2. Mapper on Ball Mapper. This section provides a new construction of a Mapper graph, as described in Section 2.1, on the output of the Ball Mapper, described in Section 2.2.

Note that the Mapper construction is based on a cover \mathcal{C} of the range of the lens function $f : X \rightarrow \mathbb{R}^n$. Typically $n = 1$ or is a small number, as the range of f needs to be covered with a collection of overlapping intervals. If we want to have k intervals in each direction, we end up with k^n cover elements which is not feasible for large values of n . However, lens functions having ranges in \mathbb{R}^n , for large value of n , are more likely to preserve important information about the high dimensional dataset X . To be able to use such a function in the Mapper construction, we introduce a new method of Topological Data Analysis to understand the shape of X when the range n of the considered lens function is relatively large. We note that in this case $f(X)$ alone is a point cloud and the Ball Mapper construction can be applied to it. Note that the Ball Mapper provides an overlapping, adaptive cover of $f(X)$ that can be used in the Mapper algorithm.

In a more general setting the presented method can be applied to analyze two point clouds PC_1 and PC_2 that are related by a function $p : PC_1 \rightarrow PC_2$. Our goal is to get an insight into the first point cloud PC_1 . For that purpose, we propose the following pipeline:

- Start with PC_1 and map it via p to PC_2
- For a given choice of ϵ apply the Ball Mapper to PC_2 to obtain BM_1 and denote its clusters by $\{B(l, \epsilon)\}_{l \in L}$
- Apply a clustering algorithm of your choice to each of $\{p^{-1}(B(l, \epsilon) \cap f(PC_1))\}_{l \in L}$ to obtain a cover of PC_1
- Take the 1-dimensional nerve of the obtained cover. The obtained Mapper graph will be referred to as MoBM graph

The only two parameters of this model are the radius ϵ and the choice of the clustering algorithm. There is no need to define the number of intervals or the overlapping percentage as in the conventional Mapper; the covering of PC_2 is completely determined by the Ball Mapper graph. Note however that potentially different Ball Mapper graphs can be obtained by varying the selection of landmark points. That in practice can be obtained by permuting the points of PC_2 . An idea of the presented construction is shown at the Figure 6.

4.3. Mapper-based visualization of functions. Standard construction of Mapper or Ball Mapper for a point cloud X with a metric $d : X \times X \rightarrow \mathbb{R}^{\geq 0}$ provides a model of the point cloud X . If the point cloud X is equipped with a function $f : X \rightarrow \mathbb{R}$, an induced function \hat{f} can be defined on Mapper or Ball Mapper graph G as explained in Sections 2.1 and 2.2. This way, Mapper and Ball Mapper graphs can be used to visualize functions $f : \mathbb{R}^n \rightarrow \mathbb{R}$, where f is defined on $X \subset \mathbb{R}^n$.

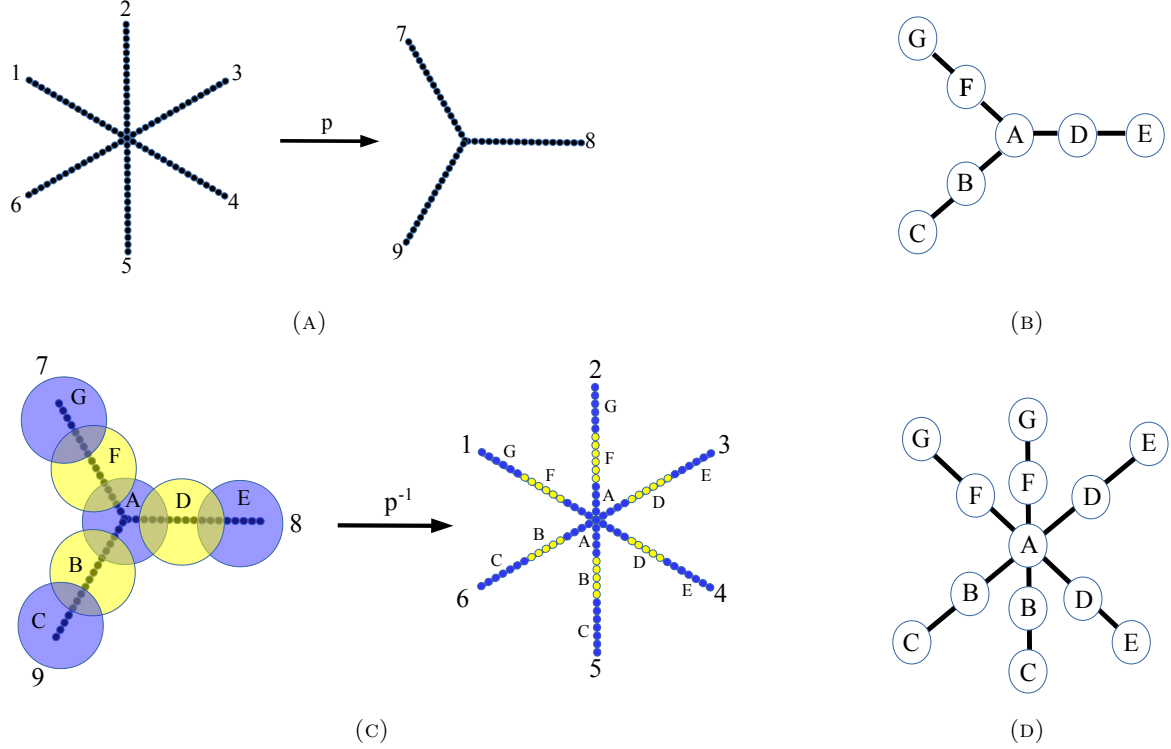


FIGURE 6. An illustration of Mapper on Ball Mapper construction. On the panel (A) the set X is given. It is mapped via the map p to the set Y . The Ball Mapper graph obtained from Y is depicted on the panel (B). Then taking the pull-back of the balls into the set X , an overlapping cover of X , presented in panel (C) arises. The corresponding Mapper (on Ball Mapper) graph is presented in panel (D).

Consider a more general question of using Mapper and Ball Mapper to visualize functions $f : \mathbb{R}^n \rightarrow \mathbb{R}^m$ for larger values of m and n . Assume that we are given $X \subset \mathbb{R}^n$ and $Y \subset \mathbb{R}^m$ and a relation $f \subset X \times Y$ (note that a function is a particular case of such a relation).

In this instance we focus on Ball Mapper-based construction. A construction for Mapper is analogous. In the first step, let us build a Mapper graphs $G(X)$ and $G(Y)$ corresponding to point clouds X and Y . Given a relation $f \subset X \times Y$ assigning points from X to the points from Y , define a map $\tilde{f} : G(X) \rightarrow G(Y)^{[0,1]}$, where $G(Y)^{[0,1]}$ denotes a set of functions from $G(Y)$ to $[0, 1]$, in the following way: For every v , vertex in $G(X)$, corresponding to a ball $B(l_X, \epsilon_X)$ compute $f(B(l_X, \epsilon_X) \cap X) \subset Y$. For every vertex v_l in $G(Y)$ corresponding to a ball $B(l_Y, \epsilon_Y)$, compute $\frac{|f(B(l_X, \epsilon_X) \cap X) \cap f(B(l_Y, \epsilon_Y) \cap Y)|}{|B(l_Y, \epsilon_Y) \cap Y|}$. This fraction indicate the percentage of points in $B(l_Y, \epsilon_Y) \cap Y$ that are in the image of the points covered by the vertex v_l in $G(X)$. When computed for every vertex in $G(X)$ this fraction gives us a coloring function on $G(Y)$ that indicates where the image of v_l is mapped.

Described construction works analogously for arbitrarily large portions, unions of vertices of the graph $G(X)$. The result of such a mapping from $G(X)$ into $G(Y)$ is a graph $G(Y)$ with the coloring function defined above. Since the coloring function has values in $[0, 1]$, we obtain $G(Y)^{[0,1]}$.

The procedure described above is automatized and a reliable interface can be found in [20]. It allows to see which regions of $G(Y)$ corresponds to chosen region of $G(X)$. By doing so, a visualization of a map $f : X \rightarrow Y$ is obtained.

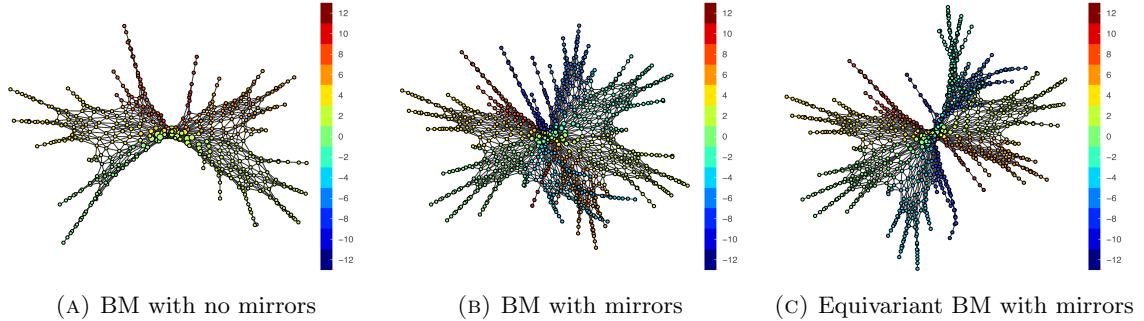


FIGURE 7. Ball Mapper applied to Jones polynomial data of knots up to 17 crossings with just one choice of a mirror (A), knots and their mirrors with the standard Ball Mapper (B) and equivariant Ball Mapper (C). Color reflects the average signature of knots in each cluster. Note that in (C) the graph is symmetric, even if the picture do not perfectly reflect this fact (it is due to the chosen subroutine to plot graphs).

5. BALL MAPPER ON KNOT POLYNOMIAL DATA

In this section we apply Ball Mapper to data obtained from Jones, Alexander, HOMFLYPT and Khovanov polynomial. The software implementing the discussed techniques and the interactive visualizations of all the plots in this paper are available at the webpage dioscuri-tda.org/BallMapperKnots.html.

5.1. Ball Mapper on the space of Jones polynomial. The aim of this section is to analyze the structure of the point cloud corresponding to the Jones polynomials of all knots with at most 17 crossings using Ball Mapper.

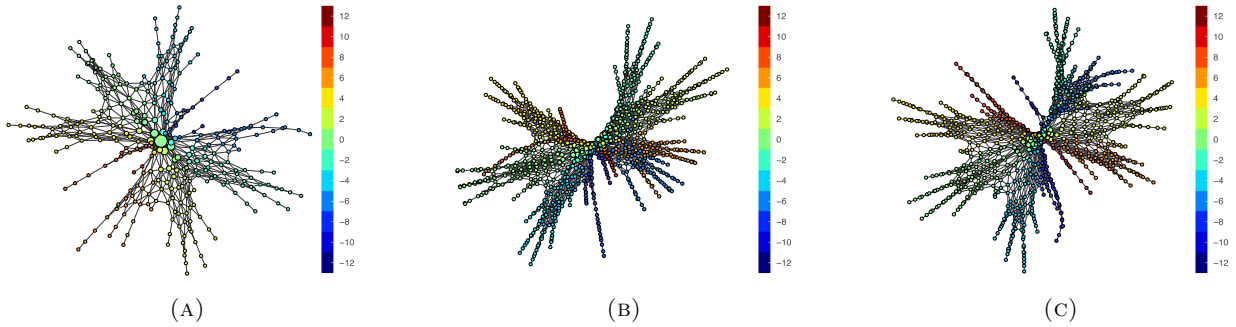


FIGURE 8. Stability of Ball Mapper approach to Jones polynomial data with respect to crossing number filtration. Ball Mapper graphs for Jones polynomial data of knots up to 15 crossings $\epsilon = 30$ with 826 nodes (A), 16 with $\epsilon = 50$ with 1008 nodes (B), 17 crossings with $\epsilon = 100$ with 890 nodes (C).

Note that our data contains knots and their mirror images, if the two are different. This choice implies that the original Jones data cloud admits central reflection symmetry with respect to the origin, see (3). Figure 7, illustrates Ball Mapper graphs on knots with just one of the mirrors included (A), knots and their mirrors standard Ball Mapper (B) and equivariant Ball Mapper construction from Section 4.1 in 7(C). The symmetry of the data is preserved by the equivariant Ball Mapper (C): for each flare there is an identical one with opposite signature, as a consequence of 4.

We need to insure that the structure of the BM graph is stable with respect to the filtration by the number of crossings, as illustrated in Figure 8 in addition to stability across the choice of parameter/radius shown as shown in Figure 9.

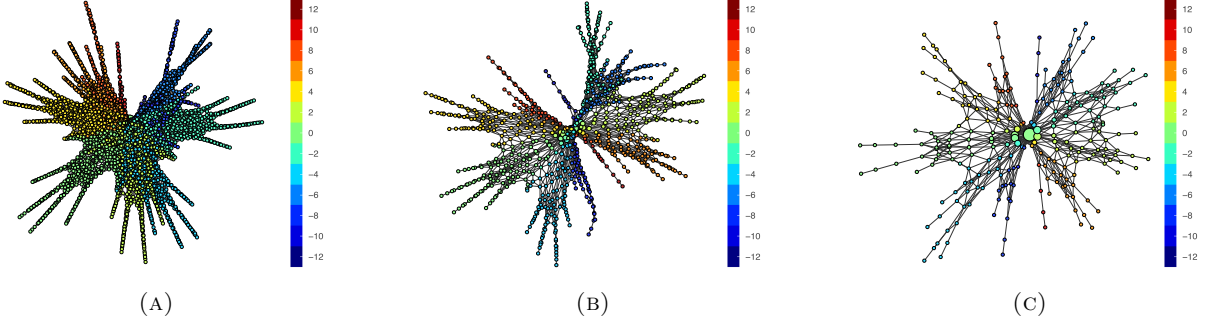


FIGURE 9. Stability of Ball Mapper approach to Jones polynomial data with respect the choice of parameter/radius ϵ . Ball Mapper graphs for Jones polynomial data of knots up to 17 crossings $\epsilon = 50$ with 3840 nodes (A), $\epsilon = 100$ with 890 nodes (B), $\epsilon = 200$ with 254 nodes (C).

With the empirical confirmation of the stability of Ball Mapper graphs on Jones polynomial data, we proceed with analyzing its star-like structure. One can observe the dense collections of nodes in the center, the majority of the knots lies in the center of the Ball Mapper graph, Figure 10(A), and there is a number of flares emanating from it. Note that the flares correspond nicely with the average value of the signature of knots in each node, Figure 10(B).

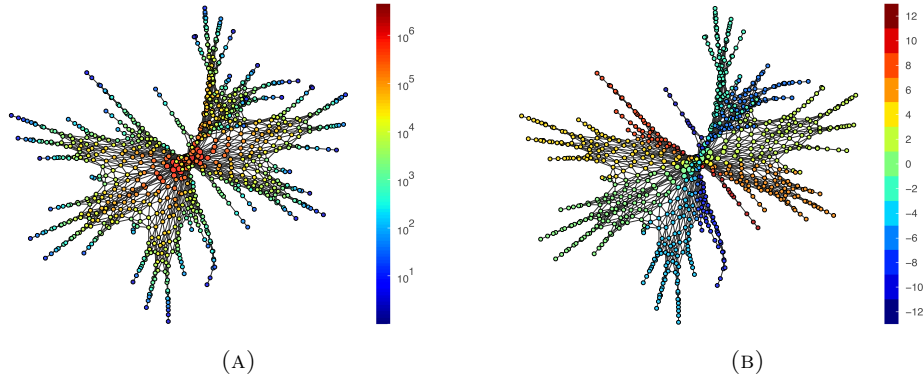


FIGURE 10. Ball Mapper graph for the Jones polynomial data of knots up to 17 crossings with color reflecting the size of the node that equals the number of knots in that cluster (A), and the average signature of knots in each cluster (B).

Additionally, Figure 11 provides evidence that nodes in the center of the Ball Mapper graph contain a mixture of alternating and non-alternating knots with a range of crossing numbers. On the other hand, flares consist mostly of the points corresponding to alternating knots with the highest crossing number.

Following up on this insight, Figure 12, shows the distribution of points corresponding to 16 crossing knots within the BM of Jones data for 17 crossing knots. In summary, 16 crossing alternating knots are underrepresented in the center and very ends of the flares while non-alternating 16 crossing knots belong to central nodes, and similar structures appear when visualizing data

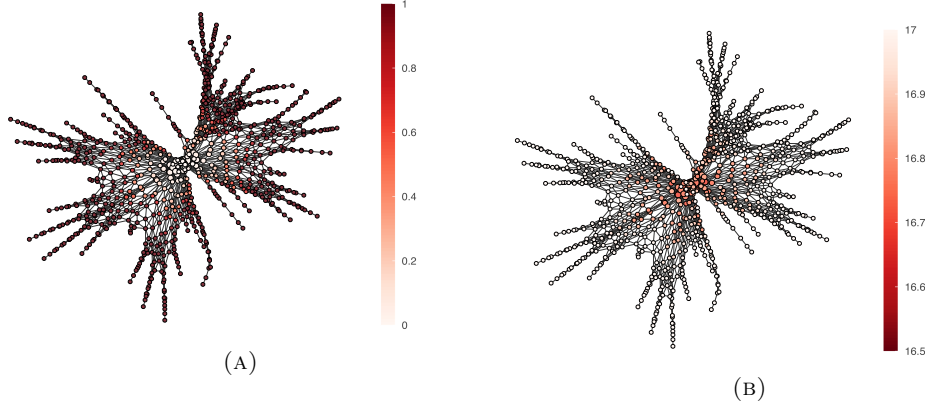


FIGURE 11. Jones space of knots of up to 17 crossings colored by the fraction of alternating knots in each cluster (A), and by the crossing number (B).

corresponding to crossing number equal to m within data of all knots with up to $n > m$ crossings for $n \leq 17$.

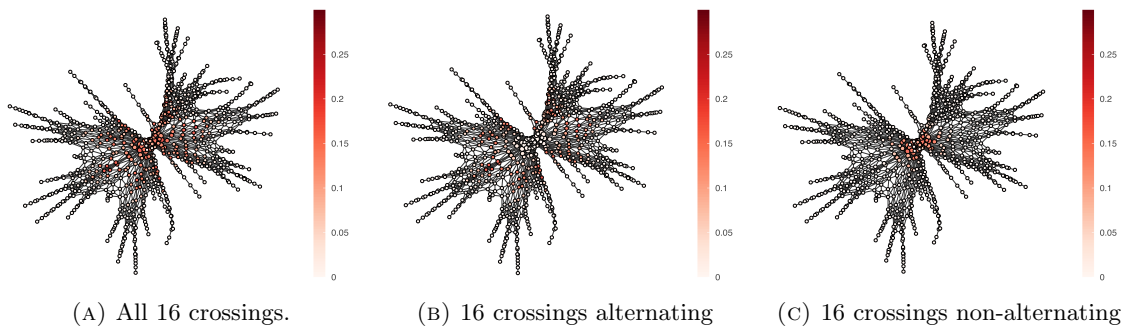


FIGURE 12. Ball Mapper graph for the Jones polynomial data of knots up to 17 crossing colored by the fraction of knots in each cluster that have exactly 16 crossings.

Interpretation of Figure 13 together with insights from Figure 10(B), suggest that all of the insights from Jones data for all knots up to 17 crossings carry over to Jones data of only alternating or just non-alternating knots with exactly 17 crossings. Their Ball Mapper graphs remain star-like with the flares correlated with signature values. The central area in the Ball Mapper of alternating knots consist of a single node containing knots with their mirror images, hence, the average signature is zero. This implies that in the Ball Mapper of all knots the non-alternating knots are concentrated in central nodes that also have smaller span and, as we can see in Figure 14, smaller norms of their Jones polynomials. Note that the flares in the Ball Mapper of non-alternating knots are less prominent in just non-alternating data.

Knots in the central nodes of Ball Mapper graphs have Jones polynomials with smaller spans and L^2 norms, and the one with high values are at ends of flares, Figure 14. Table 2 provides details of the distribution of knots with at most 17 crossings with respect to the norm of their Jones polynomials. Results in the table show that just over half of all knots have norm less than 200, quarter less than 100, $\frac{1}{12}$ th less than 50 and just not even a percent of all knots has the norm less than 20.

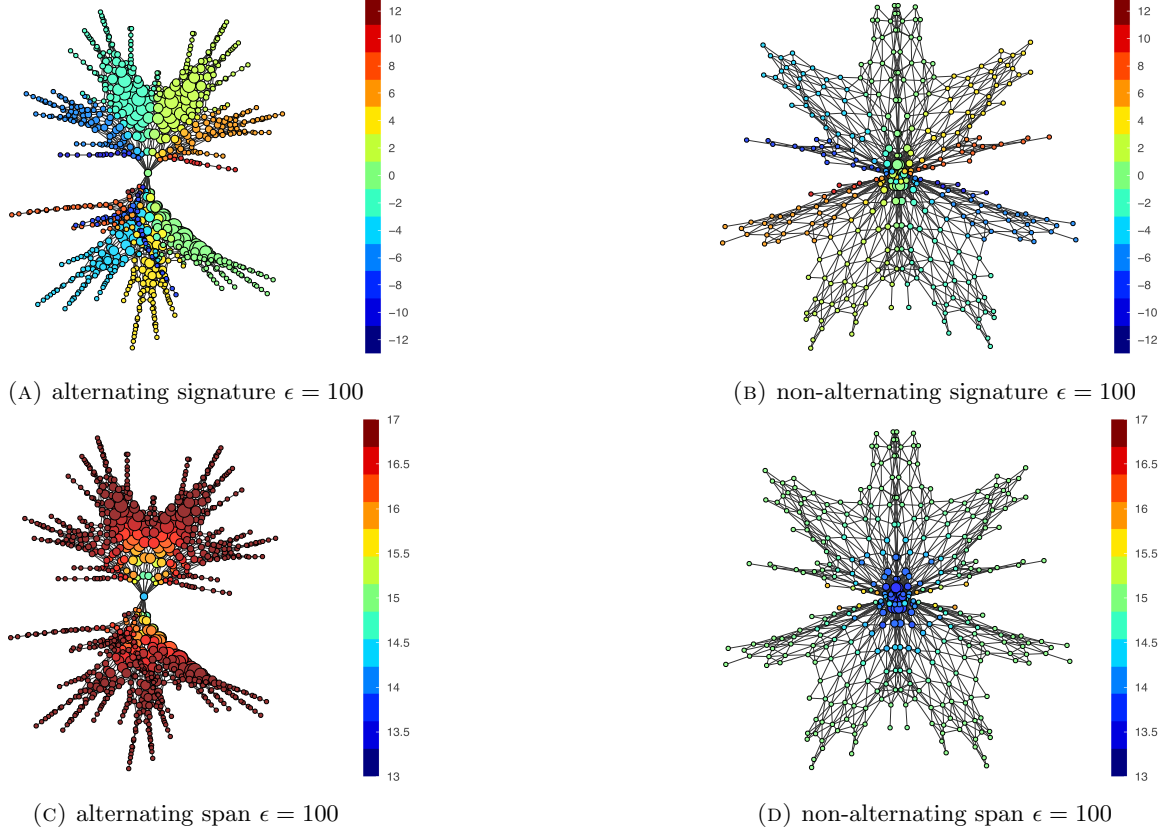


FIGURE 13. Ball Mapper for Jones polynomial data of only alternating (A), (C) and only non-alternating knots (B), (D), up to 17 colored by the signature and the span, respectively.

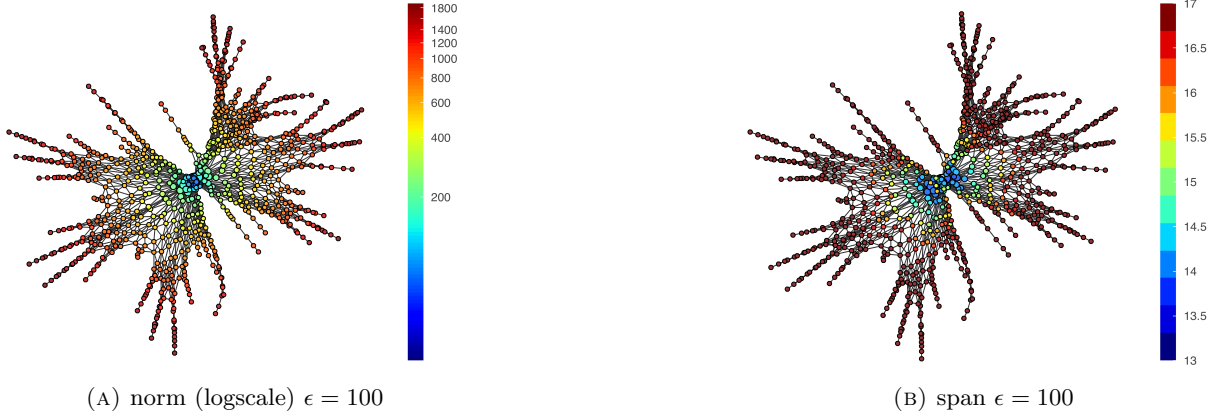


FIGURE 14. Ball Mapper of Jones polynomial data of knots up to 17 crossings colored by the norm (A) and the span of the Jones polynomial (B).

The next natural question is if filtration of the Jones polynomial data by the norm of the Jones polynomial would yield a similar structure in their Ball Mapper graphs, or informally, if we zoom into the central part of the call mapper graph will it exhibit self-similarity. Figure 15,

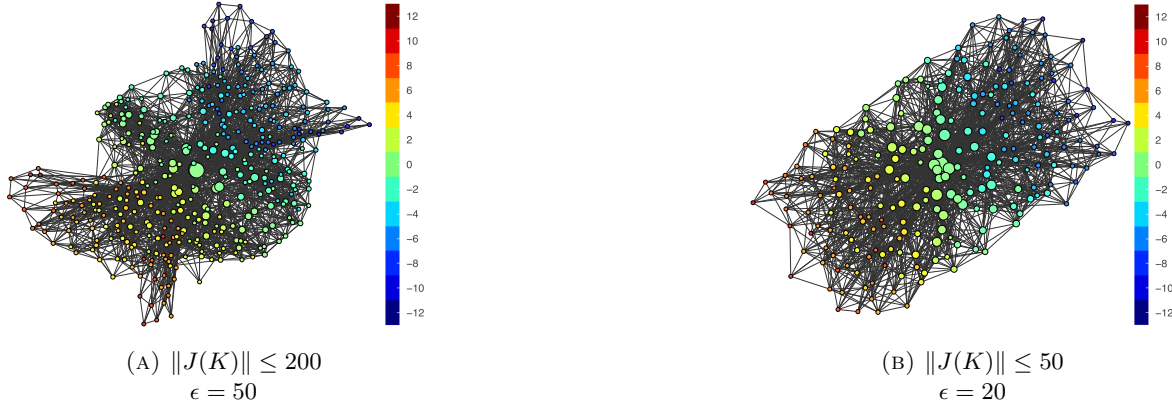


FIGURE 15. Jones up to 17 crossings with norm less than a threshold, for two different values of the threshold 200 in (A) and 50 in (B), colored by the average signature of knots in each cluster. The number of knots considered for each picture can be found in Table 2.

contains two sample Ball Mapper graphs, and indicates that while the star-like structure is not fully preserved, both Ball Mapper graphs exhibit the folklore result attributed to many that the Jones and Alexander polynomial essentially determine signature modulo 4 [11, 34].

From a theoretical point of view, the most intriguing insight originates from Figure 10(B) that suggests that the flares of the Jones data Ball Mapper graph are related with the signature. More precisely, the flares, outside of the central clusters, contain only knots with equal signature. This insight relates with the Garoufalidis conjecture, building on the following theorem [16, 18, 19].

Theorem 5.1 (Garoufalidis '03). *For all simple knots (all the roots $\alpha \in \Delta(K)$ of the Alexander polynomial where $|\alpha| = 1$ have multiplicity 1) up to 8 crossings and for all torus knots, the colored Jones polynomial determines the signature of the knot.*

Garoufalidis' conjecture was originally stated for the colored Jones polynomial and only simple knots where simple is defined in terms of the Alexander polynomial. Therefore the observation that knots at the center of the Ball Mapper graph of a Jones polynomial happen to have mixed values of signature is not an evidence against Garoufalidis' conjecture, but an indication that perhaps, in certain settings, Jones polynomial relates with signature. For Khovanov-thin classes of knots where this would be true (up to some resolution determined by the Ball Mapper parameters) it would imply that the Jones polynomial alone determines the Khovanov homology (hence the polynomial) since it is proven that the Jones polynomial and signature determine Khovanov homology for all Khovanov thin knots [38]. Khovanov thin knots include alternating and some other classes of knots such as quasi-alternating. However, in the light of the distribution of knots within the Ball Mapper graph, see Figure 10 and Table 2, Ball Mapper insights into when does the Jones polynomial "determine" signature would have limited applicability.

$\ J(K)\ \leq$	∞	200	100	50	20
No. of knots	19,510,658	9,195,232	4,540,102	1,515,886	150,808

TABLE 2. Number of knots up to 17 crossings for which the Euclidean norm of the Jones polynomial is less than a threshold value.

5.2. Ball Mapper on Alexander, HOMFLYPT, and Khovanov polynomial data. In this section we analyze sample Ball Mapper graphs for Alexander, HOMFLYPT, and Khovanov polynomial data obtained using the same approach as in Section 5.1 for knots up to 17 crossings.

Ball Mapper graph for the Alexander polynomial data has linear structure and it is stable with respect to crossing number filtration and the choice of Ball Mapper parameter as illustrated in Figure 16. The knots in the center are a mix of alternating and non-alternating, while the ends contain high crossing alternating knots. The two flares correspond to knots with signature modulo 4 equal to zero or 2, consistent with the folklore theorem [11].

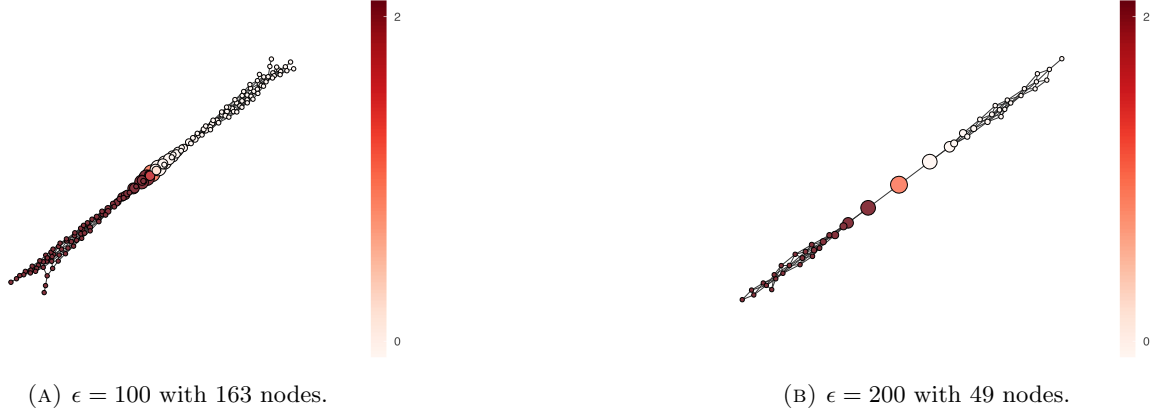


FIGURE 16. Ball Mapper graphs for Alexander polynomial data of knots up to 17 crossings colored by signature modulo 4. Note that in each picture some knots that belong to isolated nodes are omitted.

Ball Mapper graphs of HOMFLYPT of all knots up to 15 crossings for two different choices of radii colored by the average signature of knots in each node are presented in Figure 17. The analogous image for Khovanov polynomial data for non-alternating knots up to 15 crossings is shown on Figure 18. Both datasets share the star-like structure with the Ball Mapper graph of the Jones polynomial and satisfy similar properties, in particular with respect to signature.

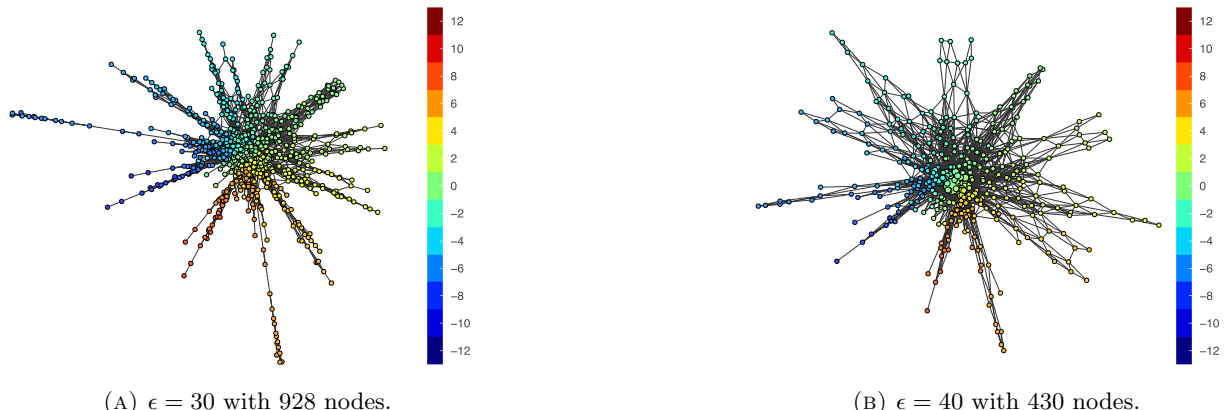
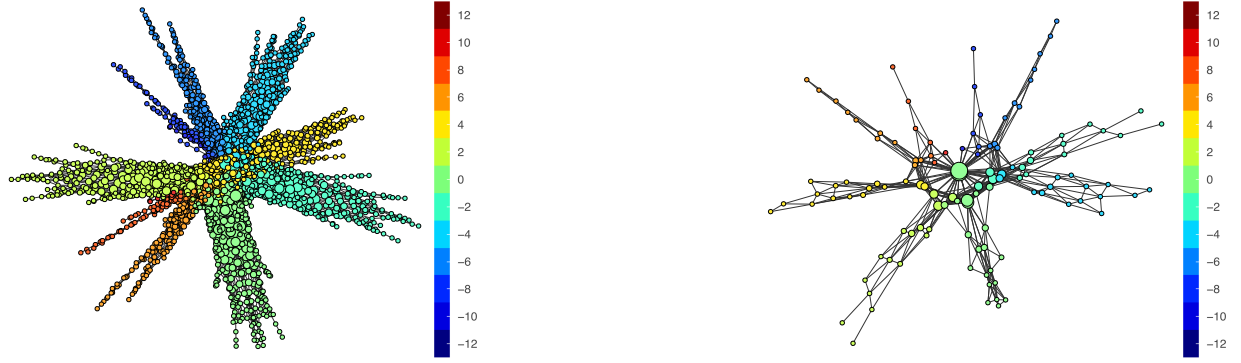


FIGURE 17. Ball Mapper for the HOMFLYPT polynomial data of knots up to 15 crossings at different radii colored by signature. Note that in each picture some knots that belong to isolated nodes are omitted.



(A) $\epsilon = 10$ with 2298 nodes.

(B) $\epsilon = 40$ with 122 nodes.

FIGURE 18. Ball Mapper graphs for Khovanov polynomial data of non-alternating knots up to 15 crossings for two different values of radius, colored by signature.

In spite of shape similarity, there are significant differences between the distribution of knots within these Ball Mapper graphs. Figure 19 shows Ball Mapper graphs of non-alternating knots up to 15 crossings for Jones, Khovanov, and HOMFLYPT data colored by the standard deviation of signature within each node. Jones and Khovanov Ball Mapper graphs exhibit much better separation of knots with different signatures than the HOMFLYPT. Weaker separation in HOMFLYPT than Jones data can be understood via specialization described in Section 2.3 that could have been detected using Mapper on Ball Mapper approach: central nodes in Jones data are pulled back to both central and nodes in the flares, see Figure 25.

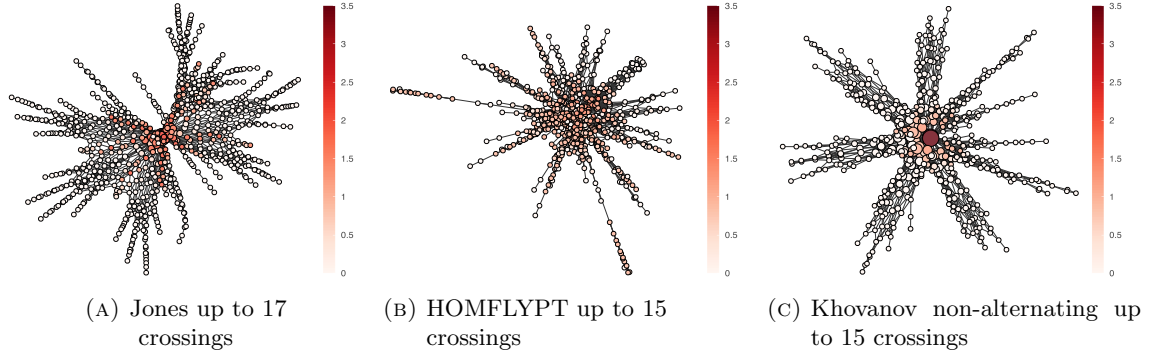


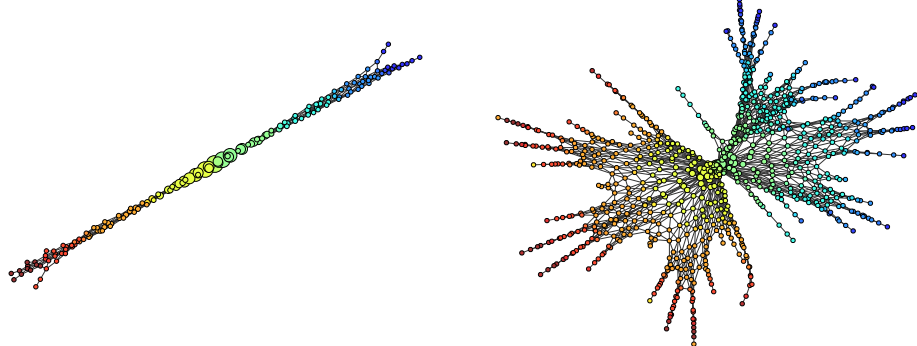
FIGURE 19. Ball Mapper graphs for different polynomials data of knots colored by the standard deviation of the signature in each cluster.

6. KNOT INVARIANTS: COMPARISONS

Section 5 provides detailed analysis of Ball Mapper graphs for Jones, Alexander, HOMFLYPT and Khovanov polynomials with respect to various numerical invariants such as crossing number, signature and binary properties such as a variable indicating if a knot is alternating.

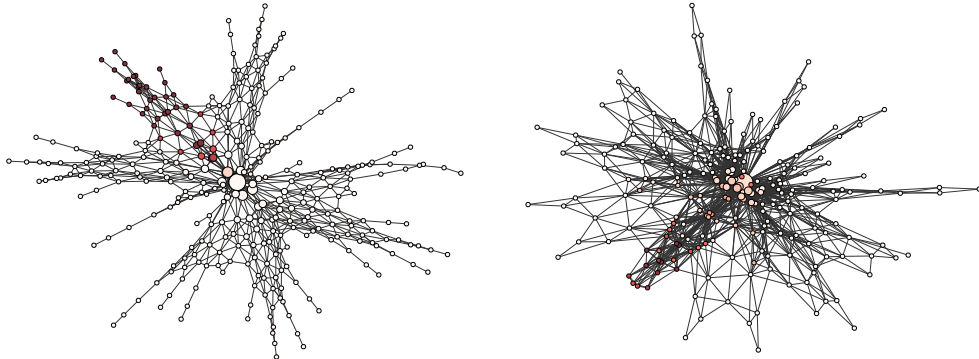
In this section, two more advanced techniques are utilized to further investigate spaces of different knot invariants in order to compare them. First, spaces of two invariants can be compared by constructing their Ball Mapper graphs and visualizing the maps between them as described in Section 4.3. Next, we use Mapper on Ball Mapper construction from Section 4.2 to investigate relative strengths of two invariants.

6.1. Ball Mapper comparisons. Visualizing functions in Section 4.3 requires two point clouds $X \subset \mathbb{R}^n$ and $Y \subset \mathbb{R}^m$ and a relation $f \subset X \times Y$ as an input. To illustrate this process we use the collection \mathcal{K} of knots up to 17 crossings and point clouds $J(\mathcal{K}) \subset \mathbb{R}^{51}$ for the Jones polynomials of knots from \mathcal{K} and $A(\mathcal{K}) \subset \mathbb{R}^{17}$ corresponding to the Alexander polynomials of knots from \mathcal{K} obtained as in Section 3.



(A) Ball Mapper graph (containing 163 nodes) of Alexander polynomial of all knots up to 17 crossings with $\epsilon = 100$. (B) Ball Mapper graph (containing 890 nodes) of Jones polynomial of all knots up to 17 crossings with $\epsilon = 100$.

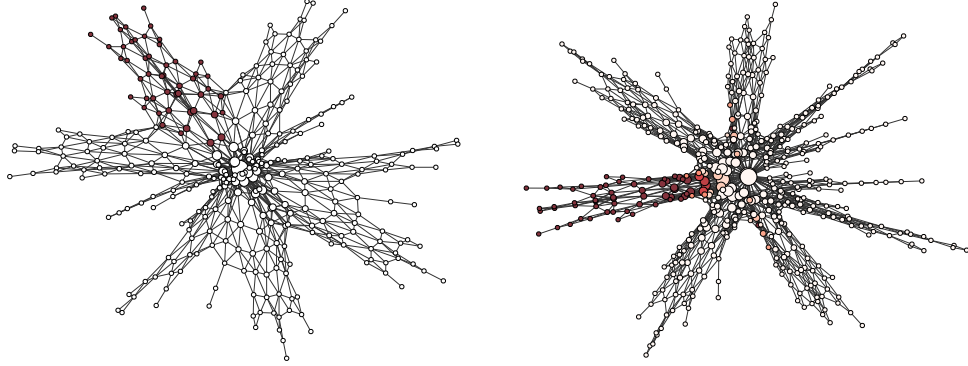
FIGURE 20. Representation of map from the space of Alexander knots up to 17 crossings and the space of Jones knots up to 17 crossings. BM custom colored to show region correspondence, i.e. regions of the same color are mapped to each other.



(A) Ball Mapper graph (containing 326 nodes) of Jones polynomial of all knots up to 15 crossings with $\epsilon = 50$. (B) Ball Mapper graph (containing 258 nodes) of HOMFLYPT polynomial of all knots up to 15 crossings with $\epsilon = 50$.

FIGURE 21. Representation of map from the space of Jones knots up to 15 crossings and the space of HOMFLYPT knots up to 15 crossings. BM custom colored to show region correspondence, i.e. regions of the same color are mapped to each other. The flare containing knots with 0 signature is highlighted.

Using the set of knots, \mathcal{K} as the common indexing set, we define the relation $f \subset A(\mathcal{K}) \times J(\mathcal{K})$ in the following way: for a given knot $K \in \mathcal{K}$ its Alexander polynomial $A(K)$ in $A(\mathcal{K})$ is related to its Jones polynomial $J(K)$ in $J(\mathcal{K})$. Note that this is a relation rather than a function, since some knots from \mathcal{K} may have the same Alexander polynomial, but different Jones polynomials,



(A) Ball Mapper graph (containing 340 nodes) of Jones polynomial of all non-alternating knots up to 15 crossings with $\epsilon = 30$. (B) Ball Mapper graph (containing 498 nodes) of Khovanov data for all non-alternating knots up to 15 crossings with $\epsilon = 20$.

FIGURE 22. Representation of map from the space of Jones non-alternating knots up to 15 crossings and the space of Khovanov non-alternating knots up to 15 crossings. BM custom colored to show region correspondence, i.e. regions of the same color are mapped to each other. In this example the region corresponding to the signature 0 flare is colored in (A).

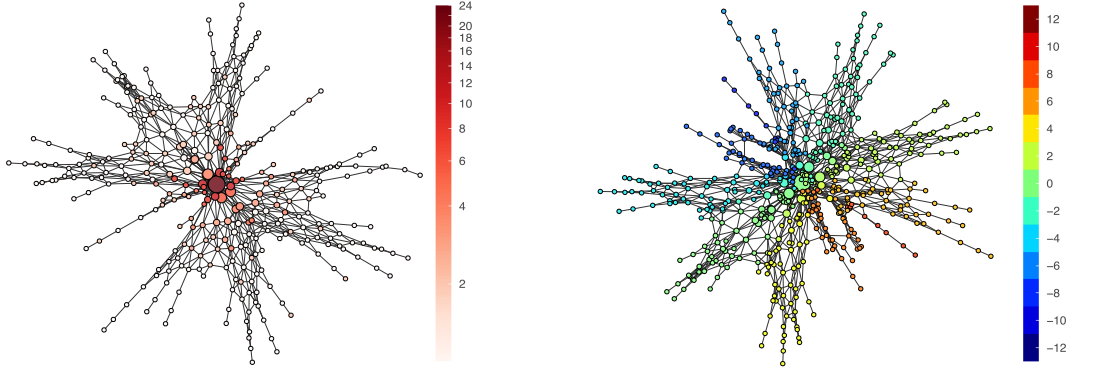
and vice versa. In this case, a single point from $A(\mathcal{K})$ can be related to multiple points of $J(\mathcal{K})$ or the other way around. Figure 20 illustrates this relation: colors indicate matching regions in the Alexander and Jones Ball Mapper graphs. Note that, roughly, the linear structure of the Alexander Ball Mapper induces the linear structure among the flares in the star-like Ball Mapper graph of the Jones data, also consistent with the signature modulo 4: one end of the Alexander Ball Mapper corresponds to it being zero and the other one to two.

6.2. Mapper on Ball Mapper for spaces of knot polynomials. The key insight for this section is the existence of algebraic relation between HOMFLYPT and both Alexander and Jones polynomial, as well as Khovanov and Jones polynomials, see Section 2.3. These specializations tie in with the framework introduced in Section 4.2 as they can be used as lenses for Mapper when using Mapper on Ball Mapper, or MoBM, construction.

In what follows, we apply Mapper on Ball Mapper to knot data using the specialization from HOMFLYPT to Alexander/Jones polynomial described in Section 2.3 as lenses and Ball Mapper on the Alexander/Jones polynomial point cloud as a coverage of the lense's range as well as the specialization from Khovanov homology to Jones polynomial described in the same section. This way we obtain Mapper on Ball Mapper structure of both HOMFLYPT and Khovanov data.

As a clustering method in MoBM construction we use the DBSCAN algorithm. DBSCAN requires parameter ϵ_{DB} in addition ϵ used in Ball Mapper construction.

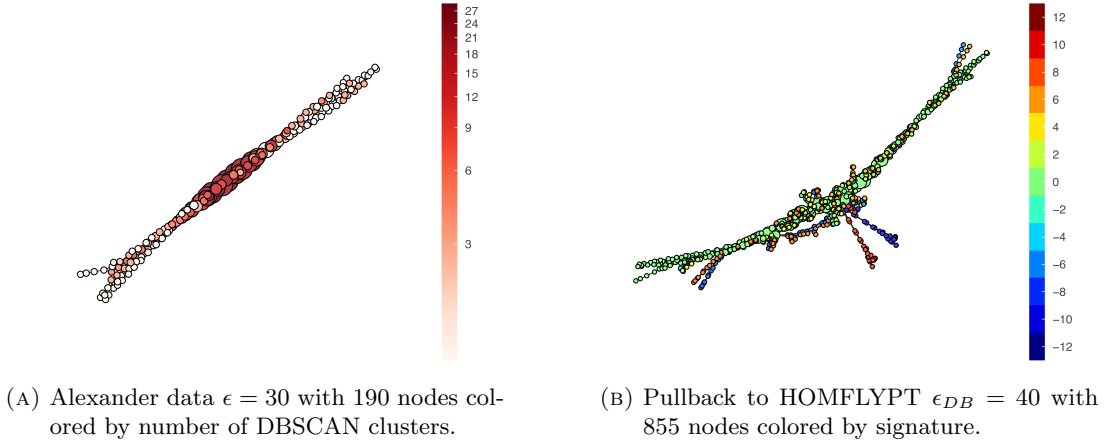
Figure 23 emphasizes similarities between the Jones and HOMFLYPT point cloud structures. The Mapper on Ball Mapper (MoBM) construction can be thought of as a transition from Jones to HOMFLYPT data that emphasizes some differences between the structures of those two datasets, see Figure 23(B). The number of nodes on Mapper on Ball Mapper graph is bigger than in the Ball Mapper graph of the Jones Ball Mapper (being the cover of the range of the lens) as indicated at the Figure 23(A). This is a consequence of the fact that pull-backs of certain nodes in the Ball Mapper graph contains more than one cluster returned by the chosen clustering method. Informally, we may say that the lenses are not injective at those regions. The nodes of Ball Mapper for the Jones polynomial that have more than one connected component in the pullback are located in the center



(A) Jones BM $\epsilon = 50$ with 326 nodes colored by the number of DBSCAN clusters .
 (B) Pullback to HOMFLY $\epsilon_{DB} = 40$ with 644 nodes.

FIGURE 23. Mapper on Ball Mapper graph on Jones-HOMFLYPT data pair. Image (A) shows Ball Mapper graph for Jones data for knots up to 15 crossings at $\epsilon_{BM} = 50$ with a total of 326 nodes. Images (B) show Mapper on Ball Mapper construction obtained from (A) and the HOMFLYPT data for values of the parameter 40 for the DBSCAN clustering algorithm colored by signature.

of the Jones Ball Mapper graph, see Figure 23(A). This is where, intuitively, HOMFLYPT provides a better distinction between knots than the Jones polynomial.



(A) Alexander data $\epsilon = 30$ with 190 nodes colored by number of DBSCAN clusters.
 (B) Pullback to HOMFLYPT $\epsilon_{DB} = 40$ with 855 nodes colored by signature.

FIGURE 24. Mapper on Ball Mapper procedure from Alexander to HOMFLYPT polynomial data for all knots up to 15 crossings.

Figure 24 illustrates the HOMFLYPT structure obtained from the pull back of the linear structure of the Ball Mapper graph for the Alexander polynomial. In this case, we are using Ball Mapper graph of Alexander data obtained for $\epsilon = 100$. As the parameter ϵ_{DB} decreases in the Figure 24(B), (C), and (D), additional "flares" that contain knots with the same signature appear. However, notice that this is not the star-like structure featured in Ball Mapper graph of the HOMFLYPT data on Figure 17 or Mapper on Ball Mapper construction on Jones-HOMFLYPT point clouds Figure 23. Figure 24(B) shows that the linear backbone of the Mapper on Ball Mapper graph contains knots together with their mirror images (since the average signature of those clusters is zero) but

also that the flares appear to be paired according to two different signs of the signature. For example orange-light blue that correspond to absolute value of the signature equal to 4 and red-blue flares where signature is equal to ± 10 .

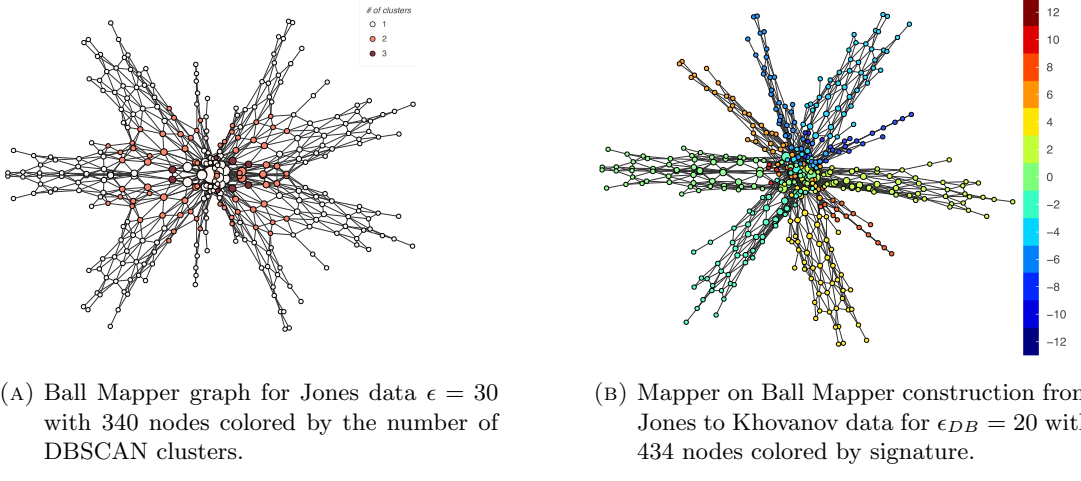


FIGURE 25. Mapper on Ball Mapper procedure from Jones to Khovanov for all non-alternating knots up to 15 crossings.

Figure 25 depicts the Mapper on Ball Mapper procedure from Jones to Khovanov data for all non-alternating knots up to 15 crossings. Figure 25(A) highlights the nodes in the Ball Mapper graph of the Jones polynomial data for which the mapping is not trivial i.e. those that are pulled to more than one node in Khovanov data. Such nodes are the ones that are in between two flares thus containing knots with different signatures. The Mapper on Ball Mapper procedure is successful in identifying the clusters in these nodes leading to a better separation of the flares than in Ball Mapper construction as shown in Figure 25(B).

REFERENCES

- [1] Cypari2 - interface to the pari library. URL: <https://cypari2.readthedocs.io>, Current Month Current Year.
- [2] James W Alexander. Topological invariants of knots and links. *Transactions of the American Mathematical Society*, 30(2):275–306, 1928.
- [3] Akram Alishahi. Unknotting number and Khovanov homology. *Pacific J. Math.*, 301(1):15–29, 2019.
- [4] Akram Alishahi and Nathan Dowlin. The Lee spectral sequence, unknotting number, and the Knight Move Conjecture. *Topology Appl.*, 254:29–38, 2019.
- [5] Akram Alishahi and Nathan Dowlin. The Lee spectral sequence, unknotting number, and the Knight Move Conjecture. *Topology Appl.*, 254:29–38, 2019.
- [6] Dror Bar-Natan, Scott Morrison, and et al. The Knot Atlas, 2011–2019. <http://katlas.org>.
- [7] Benjamin A. Burton, Ryan Budney, William Pettersson, et al. Regina: Software for low-dimensional topology. <http://regina-normal.github.io/>, 1999–2017. <http://regina-normal.github.io>.
- [8] Benjamin A. Burton. The next 350 million knots. <http://regina-normal.github.io/data.html>, 2018. <http://regina-normal.github.io/data.html>.
- [9] Jason Cantarella, Harrison Chapman, and Matt Mastin. Knot probabilities in random diagrams. *Journal of Physics A: Mathematical and Theoretical*, 49(40):405001, 2016.
- [10] Carmen Caprau, Nicolle González, Christine Ruey Shan Lee, Adam M Lowrance, Radmila Sazdanović, and Melissa Zhang. On khovanov homology and related invariants. *arXiv preprint arXiv:2002.05247*, 2020.
- [11] John H Conway. An enumeration of knots and links, and some of their algebraic properties. In *Computational problems in abstract algebra*, pages 329–358. Elsevier, 1970.
- [12] Oliver T Dasbach and Adam M Lowrance. Turaev genus, knot signature, and the knot homology concordance invariants. *Proceedings of the American Mathematical Society*, pages 2631–2645, 2011.

- [13] Yuanan Diao, Nicholas Pippenger, and De Witt Sumners. On random knots. *Journal of Knot Theory and its Ramifications*, 3(03):419–429, 1994.
- [14] Claus Ernst and DW Sumners. The growth of the number of prime knots. In *Mathematical Proceedings of the Cambridge Philosophical Society*, volume 102, pages 303–315. Cambridge University Press, 1987.
- [15] Peter Freyd, David Yetter, Jim Hoste, WB Raymond Lickorish, Kenneth Millett, and Adrian Ocneanu. A new polynomial invariant of knots and links. *Bulletin (new series) of the American mathematical society*, 12(2):239–246, 1985.
- [16] Stavros Garoufalidis. Does the jones polynomial determine the signature of a knot? *arXiv preprint math/0310203*, 2003.
- [17] Stavros Garoufalidis. A conjecture on khovanov’s invariants. *Fundamenta Mathematicae*, 184:99–101, 2004.
- [18] Stavros Garoufalidis and Thang TQ Lê. The colored Jones function is q-holonomic. *Geometry & Topology*, 9(3):1253–1293, 2005.
- [19] Stavros Garoufalidis and Martin Loeb. A non-commutative formula for the colored Jones function. *Mathematische Annalen*, 336(4):867, 2006.
- [20] Davide Gurnari. Knots bm. URL: <https://github.com/dgurnari/knotsBM>, August 2021.
- [21] Davide Gurnari. Knots data. URL: <https://cloud.impan.pl/s/XEdAp6bHPGJHnEy>, August 2021.
- [22] Jim Hoste. The enumeration and classification of knots and links. In *Handbook of knot theory*, pages 209–232. Elsevier, 2005.
- [23] Jim Hoste, Morwen Thistlethwaite, and Jeff Weeks. The first 1,701,936 knots. *The Mathematical Intelligencer*, 20(4):33–48, 1998.
- [24] Mark C Hughes. A neural network approach to predicting and computing knot invariants. *arXiv preprint arXiv:1610.05744*, 2016.
- [25] Slavik V Jablan and Sazdanovic Radmila. *Linknot: knot theory by computer*, volume 21. World Scientific, 2007.
- [26] Vishnu Jejjala, Arjun Kar, and Onkar Parrikar. Deep learning the hyperbolic volume of a knot. *arXiv preprint arXiv:1902.05547*, 2019.
- [27] Vaughan F. R. Jones. A polynomial invariant for knots via von Neumann algebras. *Bull. Amer. Math. Soc. (N.S.)*, 12(1):103–111, 1985.
- [28] Louis H Kauffman and Laurence R Taylor. Signature of links. *Transactions of the American Mathematical Society*, 216:351–365, 1976.
- [29] Mikhail Khovanov. A categorification of the jones polynomial. *Duke Math. J.*, 101(3):359–426, 2000.
- [30] Jesse SF Levitt, Mustafa Hajij, and Radmila Sazdanovic. Big data approaches to knot theory: Understanding the structure of the jones polynomial. *arXiv preprint arXiv:1912.10086*, 2019.
- [31] WB Raymond Lickorish. *An introduction to knot theory*, volume 175. Springer Science & Business Media, 2012.
- [32] Charles Livingston. *Knot theory*, volume 24. Cambridge University Press, 1993.
- [33] Dłotko Paweł. Ball mapper: a shape summary for topological data analysis. *arXiv:1901.07410*, 2019.
- [34] Józef H Przytycki and Paweł Traczyk. Invariants of links of conway type. *arXiv preprint arXiv:1610.06679*, 2016.
- [35] Jacob Rasmussen. Khovanov homology and the slice genus. *Inventiones mathematicae*, 182(2):419–447, 2010.
- [36] Dale Rolfsen. Knots and links, volume 346. h, 2003.
- [37] Alex Shumakovitch. Private communication, 2019.
- [38] Alexander N Shumakovitch. Torsion of the khovanov homology. *arXiv preprint math/0405474*, 2004.
- [39] Gurjeet Singh, Facundo Memoli, and Gunnar Carlsson. Topological methods for the analysis of high dimensional data sets and 3d object recognition. 2007.
- [40] Matt Ward. Using neural networks to classify knots: Data mining and deep learning in knot theory. 2018.

DIOSCURI CENTRE IN TOPOLOGICAL DATA ANALYSIS, MATHEMATICAL INSTITUTE, POLISH ACADEMY OF SCIENCES, WARSAW, POLAND

Email address: pdlotko@impan.pl

DIOSCURI CENTRE IN TOPOLOGICAL DATA ANALYSIS, MATHEMATICAL INSTITUTE, POLISH ACADEMY OF SCIENCES, WARSAW, POLAND

Email address: dgurnari@impan.pl

DEPARTMENT OF MATHEMATICS, NORTH CAROLINA STATE UNIVERSITY, RALEIGH, NC

Email address: rsazdanovic@math.ncsu.edu